Adaptive scheme based on entropy production: robustness through severe test cases for hyperbolic conservation laws

Mehmet Ersoy, Frederic Golay, Lyudmyla Yushchenko

Adaptive scheme based on entropy production: robustness through severe test cases for hyperbolic conservation laws.

Mehmet Ersoy*[1], Frédéric Golay†[1], and Lyudmyla Yushchenko‡[1]

[1] Université de Toulon, IMATH, EA 2134, 83957 La Garde, France.

December 13, 2013

Contents

1 Introduction **2**

2 The 1D gas dynamics equations **3**

3 The adaptive numerical scheme **4**

4 Numerical results **6**
4.1 Test 1: a modified version of the Sod's shock tube problem 7
4.2 Test 2: a modified 123 problem 10
4.3 Test 3: the left half of the blast wave of Woodward and Colella 13
4.4 Test 4: the Two Shock Riemann problem 16
4.5 Test 5: a modified Leblanc test problem 19
4.6 Test 6: the blast wave problem 23

5 Concluding remarks and perspectives **26**

Abstract

In this paper, we study the robustness of the 1D adaptive numerical scheme based on numerical density of entropy production for hyperbolic conservation. In particular, we focus on vacuum states or low densities states or both in presence of strong shocks solutions to the one-dimensional gas dynamics equations for ideal gas. To this purpose, it is numerically shown that the adaptive numerical scheme is well-designed to capture accurately these type of solutions as the pressure vanishes. The efficiency of the scheme is investigated through several test cases for first and second order scheme with a MUSCL reconstruction. We focus in particular on several numerical experiments to test the ability to conserve the entropy in the adaptive framework, to capture strong discontinuities (both shocks and contact discontinuities) as well as strong rarefactions. We also perform some numerical test case for solutions which are close to the vacuum or vanishes.

Keywords: hyperbolic system, finite volume scheme, local mesh refinement, numerical density of entropy production, local time stepping, low density, vacuum state, strong shock, strong contact discontinuities, strong rarefaction

* *Mehmet.Ersoy@univ-tln.fr*
† *Frederic.Golay@univ-tln.fr*
‡ *Lyudmyla.Yushchenko@univ-tln.fr*

1 Introduction

We are interested in the computation of numerical entropy solutions containing vacuum states or low densities states for hyperbolic conservation laws:

$$\left\{ \begin{array}{ll} \dfrac{\partial \boldsymbol{w}}{\partial t} + \dfrac{\partial \boldsymbol{f}(\boldsymbol{w})}{\partial x} = 0, & (t,x) \in \mathbb{R}^+ \times \mathbb{R} \\ \boldsymbol{w}(0,x) = \boldsymbol{w}_0(x), & x \in \mathbb{R}. \end{array} \right. \tag{1}$$

where $\boldsymbol{w} : \mathbb{R}^+ \times \mathbb{R} \to \mathbb{R}^d$ stands for the vector state and $\boldsymbol{f} : \mathbb{R}^d \to \mathbb{R}^d$ the flux function.

It is well-known that solutions of System (1) can and will breakdown at a finite time, even if the initial data are smooth, and develop complex structure (shock wave interactions). In such a situation, the uniqueness of the (weak) solution is lost and is recovered by completing System (1) with an entropy inequality of the form:

$$\frac{\partial s(\boldsymbol{w})}{\partial t} + \frac{\partial \psi(\boldsymbol{w})}{\partial x} \leq 0 \ , \tag{2}$$

where (s, ψ) stands for a convex entropy-entropy flux pair. This inequality allows to select the physical relevant solution. Moreover, the entropy satisfies a conservation equation only in regions where the solution is smooth and an inequality when the solution develops shocks. In simple cases, it can be proved that the term missing in (2) to make it an equality is a Dirac mass.

In particular, solving Equation (1) in presence of low density state or vacuum state or in presence of a strong shock also constitute a source of difficulties in regard to uniqueness of solutions to the Riemann problem. The vacuum states introduces an indeterminacy in the variables which describe the flow (vacuum has zero energy, momentum and pressure and the velocity is not defined since $u = q/\rho$ where q stands for the momentum) while low density state often yields to numerical instabilities. Strong shocks induce a large discontinuity in the pressure and often one has to impose limitations on the strength of shocks from mathematical as well as numerical viewpoint (see e.g. [12, 15, 3]). In general, it often yields singularities in the physical systems producing mathematical ill-posedness and numerical instabilities for solutions which are close to those states. We refer to [16, 2, 8, 9, 13, 3] for mathematical discussions about those states. As a consequence, to compute accurately such type of solutions is a challenging problem that we intend to implement efficiently in a multi-scale adaptive framework.

Following Ersoy *et al* [5] and the above considerations, we will numerically investigate the robustness of the adaptive numerical scheme through the computation of those solutions. Let us recall that the adaptive multi-scale scheme is based on the numerical density of the entropy production. This quantity is a measure of the amount of violation of the entropy equation (as a measure of the local residual as already pointed out in [1, 7, 11, 10, 5]). Thus, the numerical density of entropy production provides information on the need to locally refine the mesh (e.g. if the solution develops discontinuities) or to coarsen the mesh (e.g. if the solution is smooth and well-approximated). We have shown that for solutions far from those states, such indicator is able (see Ersoy *et al* [5]) not only to provide an efficient *a posteriori* error, but also to reproduce the qualitative structure of the solution and to pilot the adaptive scheme. Let us also emphasize that we prefer to use the classical Godunov solver instead of linearized or approximated solver in the finite volume framework. Indeed, it may happen for data close to the vacuum state or in situations where there is a strong expansion, those linearized scheme fail (see for instance, citeEMRS91,leveque2002,Toro09).

The paper is organized as follows. In Section 2, we fix notations and we recall the one dimensional gas dynamics equations for perfect gas. In section (3), we recall the finite volume approximation in the multi-scale adaptive framework as introduced by Ersoy *et al* [5]. Moreover, we recall the procedure to deal with solutions close to vacuum states. Finally, in Section 4, through several numerical test case, we show the efficiency of the present numerical scheme for solutions which are close to vacuum state or/and in presence of strong discontinuities and rarefactions. In particular, we numerically show that those solutions are very well-computed. To illustrate this statement, we study the qualitative behavior of the adaptive numerical scheme with respect to the L^1 error norm providing quantitative results. We only restrict ourselves to solutions which are only C^0 and even with strong discontinuities as for shock or contact discontinuities since

for smooth solutions we recover the order p for a numerical scheme of order p. Even in presence of severe test cases, we emphasize that the present scheme is super-convergent or at least of order 1. We focus on the following tests:

- a modified Sod test problem,
- a 123 problem,
- a left half of the blast wave of Woodward and Colella,
- a Two shock Riemann problem,
- a modified Leblanc test case,
- a blast wave problem of Woodward and Colella

to assess the ability to conserve the entropy inequality at the discrete level, the performance of the scheme for low density flows and the robustness of the numerical method. One can found other test cases for the one dimensional gas dynamics equation for perfect gas, for instance, in [21, 20, 4, 6, 18].

2 The 1D gas dynamics equations

Let us consider a compressible perfect fluid confined in a domain $\otimes$. The governing equations for the motion of the compressible fluid in $[0,T]\times\otimes$ are the so called Euler equations

$$\left\{\begin{array}{rcl} \dfrac{\partial\rho}{\partial t}+\dfrac{\partial\rho u}{\partial x} &=& 0,\\ \dfrac{\partial\rho u}{\partial t}+\dfrac{\partial\left(\rho u^2+p\right)}{\partial x} &=& 0,\\ \dfrac{\partial\rho E}{\partial t}+\dfrac{\partial\left(\rho E+p\right)u}{\partial x} &=& 0 \end{array}\right. \tag{3}$$

where ρ is the density, $p=(\gamma-1)\rho\varepsilon$ is the pressure, u the velocity and E the total energy defined by:

$$E=\varepsilon+\frac{u^2}{2}\ .$$

Here, ε stands for the internal specific energy and γ is the ratio of the specific heats.

Making use of the notations

$$\boldsymbol{w}=\left(\begin{array}{c}\rho\\ \rho u\\ \rho E\end{array}\right),\quad f(\boldsymbol{w})=\left(\begin{array}{c}\rho u\\ \rho u^2+p\\ (\rho E+p)\,u\end{array}\right)$$

for the conservative variables and the conservative flux, the system (3) is written as a system of conservation laws (1). We complete System (3) with the entropy inequality (2) where the convex entropy $s(\boldsymbol{w})$ and the entropy flux pair $\psi(\boldsymbol{w})$ are classically given by the following relations:

$$s(\boldsymbol{w})=-\rho\ln\left(\frac{p}{\rho^\gamma}\right),\quad \psi(\boldsymbol{w})=u\,s(\boldsymbol{w})\ . \tag{4}$$

Let us note that even if System (3) is strictly hyperbolic on the set $\{\rho>0\}$, the previous quantities (4) make a sense for $\rho\geqslant 0$.

3 The adaptive numerical scheme

For the sake of completeness, we recall in this section, the first order adaptive multi scale scheme based on numerical density of entropy production for conservation laws introduced by the authors in [5]. Interested reader can found the details of the second order scheme with MUSCL reconstruction as well as the second order Adams-Bashforth time integration in [5].

One-dimensional finite volume formulation.

We recall here the well-known construction of a numerical approximation of the general non linear hyperbolic conservation laws (1)

The computational domain is split into control volumes $C_k = \left]x_{k-1/2}, x_{k+1/2}\right[$ of mesh size h_k with $x_{k\pm1/2} = x_k \pm h_k/2$. The unknowns $\boldsymbol{w}(t,x)$ are approximated by their mean values on the cell C_k at time t:

$$\boldsymbol{w}_k(t) \simeq \frac{1}{h_k}\int_{C_k} \boldsymbol{w}\,(t,x)\;dx\,.$$

Noting, $t_{n+1} = t_n + \delta t_n$ the discrete time and Integrating (3) over each strip $(t_n, t_{n+1}) \times C_k$ and applying the Green's formula we obtain:

$$\frac{\boldsymbol{w}_k^{n+1} - \boldsymbol{w}_k^n}{\delta t_n} + \frac{\delta \boldsymbol{F}_k^n}{h_k} = 0\;, \tag{5}$$

with

$$\delta \boldsymbol{F}_k^n := \boldsymbol{F}_{k+1/2}^n - \boldsymbol{F}_{k-1/2}^n$$

where $\boldsymbol{F}_{k\pm1/2}^n$ stands for the numerical fluxes at the interface $x_{k\pm1/2}$.

We use here the Godunov solver, i.e. we defined

$$\boldsymbol{F}_{k\pm1/2}^n(\boldsymbol{w}_k^n, \boldsymbol{w}_{k+1}^n) = \boldsymbol{f}\left(\boldsymbol{R}(0^{\pm}, \boldsymbol{w}_k^n, \boldsymbol{w}_{k+1}^n)\right)$$

where $\boldsymbol{f}(\boldsymbol{R}(0^{\pm}, \boldsymbol{w}_L, \boldsymbol{w}_R))$ is determined from the exact solution $\boldsymbol{R}(0^{\pm}, \boldsymbol{w}_L, \boldsymbol{w}_R)$ of the Riemann problem associated with the left $\boldsymbol{w}_L$ and the right $\boldsymbol{w}_R$ state:

$$\left\{\begin{array}{l} \dfrac{\partial \boldsymbol{w}}{\partial t} + \dfrac{\partial \boldsymbol{f}(\boldsymbol{w})}{\partial x} = 0\;, \\ \boldsymbol{w}_0(x) = \left\{\begin{array}{ll} \boldsymbol{w}_L & \text{if } x < 0\;, \\ \boldsymbol{w}_R & \text{if } x > 0\;. \end{array}\right. \end{array}\right. \tag{6}$$

In the same way, the discretization of the entropy inequality (4) yields to:

$$S_k^n := \frac{s(\boldsymbol{w}_k^{n+1}) - s(\boldsymbol{w}_k^n)}{\delta t_n} + \frac{\delta \psi_k^n}{h_k} \tag{7}$$

where

$$\delta\psi_k^n := \psi_{k+1/2}^n - \psi_{k-1/2}^n := \psi\left(\boldsymbol{R}(0^-, \boldsymbol{w}_k^n, \boldsymbol{w}_{k+1}^n)\right) - \psi\left(\boldsymbol{R}(0^+, \boldsymbol{w}_{k-1}^n, \boldsymbol{w}_k^n)\right)\;.$$

The quantity S_k^n defines the so-called numerical density of entropy production and the value

$$\mathcal{P} = \sum_{n,k} S_k^n \delta t_n h_k\;. \tag{8}$$

is the total numerical entropy production.

Mesh refinement.

In order to compute accurately the solution of hyperbolic systems, the strategy [5] consists to use the numerical density of entropy production as a mesh refinement parameter in the following meaning.

We present here a local mesh refinement procedure driven by the numerical density of entropy production. In order to reduce the time necessary to manage the refinement, we use "macro cells" which could be refined by generating hierarchical grids. Each cell can be split in two sub-cells. We thus produce a dyadic cells graph, whose numbering (in basis 2) allows a quick computing scan to determine the adjacent cells. For the convenience of the reader, we make use of the following notations: let k_b be the index which makes reference to the macro cell numbered k and b a binary number which contains the hierarchical information of a sub-cell. In particular, the level of a sub-cell C_{k_b} is defined as the length(b) $-$ 1. For instance, a macro cell C_{k_0} of level 0 will be split into two sub-cells $C_{k_{00}}$ and $C_{k_{01}}$ of level 1. A mesh refinement example is proposed in FIGURE 1.

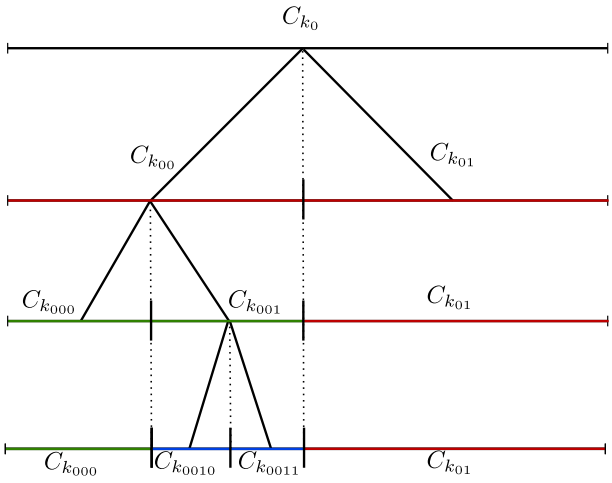

Figure 1: Example of hierarchical dyadic tree.

The mesh refinement procedure can be simply expressed as follows. We first set a mesh refinement parameter $\bar{S}$. For instance, it can be the mean value over the domain Ω at time t_n:

$$\bar{S} = \frac{1}{|\Omega|} \sum_{k_b} S^n_{k_b} \ . \tag{9}$$

We then define two coefficients $0 \leqslant \alpha_{\min} \leqslant \alpha_{\max} \leqslant 1$, which determine the ratio of numerical production of entropy leading to mesh refinement or mesh coarsening.

Thus, for each cell C_{k_b}:

- if $S^n_{k_b} > \bar{S}\alpha_{\max}$, the mesh is refined and split into two sub-cells $C_{k_{b0}}$ and $C_{k_{b1}}$,
- if $S^n_{k_{b0}} < \bar{S}\alpha_{\min}$ and $S^n_{k_{b1}} < \bar{S}\alpha_{\min}$, the mesh is coarsened into a cell C_{k_b}.

On one hand, if a cell C_{k_b} is split into two sub-cells $C_{k_{b0}}$ and $C_{k_{b1}}$, averaged values at time t_n are projected on each sub-cell (for the first order scheme):

$$\boldsymbol{w}^n_{k_{b0}} = \boldsymbol{w}^n_{k_{b1}} = \boldsymbol{w}^n_{k_b}$$

and the numerical fluxes between the two sub-cells are defined as:

$$\begin{cases} \boldsymbol{F}^n_{k_{b0}-1/2} = \boldsymbol{F}^n_{k_b-1/2} \ , \\ \boldsymbol{F}^n_{k_{b0}+1/2} = \boldsymbol{F}^n_{k_{b1}-1/2} = \boldsymbol{f}(\boldsymbol{w}^n_{k_b}) \ , \\ \boldsymbol{F}^n_{k_{b1}+1/2} = \boldsymbol{F}^n_{k_b+1/2} \ . \end{cases}$$

The adaptive mesh refinement scheme is also written in a local time stepping method to gain in time (we refer to [5] for more details).

4 Numerical results

In this section, we show the efficiency of the adaptive numerical[1] scheme based on the numerical density of entropy production through severe numerical experiments. In [5], we have pointed out that the use of the numerical density entropy production as a mesh refinement parameter is a relevant local error indicator (everywhere where the solution remains smooth) and a discontinuity detector (shocks and oscillating solutions are very well-captured). Far from large discontinuities and vacuum states, we have performed several numerical tests (the Sod's shock tube problem, the Lax's shock tube problem and the Shu-Osher test problem) and we have shown an impressive improvement with respect to uniform grids even if a large number of uniform cells are used. Moreover, the adaptive strategy, combined with a local time stepping algorithm, can significantly reduce the computational time keeping the same order of accuracy. We also refer to the 2D and 3D extension of the work [5] in [22].

From now on, we focus on severe numerical experiments designed to assess the performance of the numerical method in presence of strong discontinuities (both shocks and contact discontinuities), strong rarefactions as well as for low density flows (see for instance [17, 19, 20, 4, 18]). Therefore, in the sequel, we focus on the robustness of the present adaptive scheme.

For all test cases, numerical solutions are computed using the one-dimensional gas dynamics equations for ideal gas (3) and we make use of the following notations and settings:

Notations and settings

- In what follows, we perform several numerical tests using first and second order schemes. Thus, we will refer to AB1 as the first order scheme, AB2 as the second order Adams-Basforth scheme, RK2 as the second order Runge-Kutta scheme. AB2 and RK2 use a MUSCL reconstruction. Moreover, all computations are made with a dynamic grid except if the acronym ends with the capital letter "U" which refers to a uniform fixed grid. All computations are made with a uniform time step except if the acronym ends with the capital letter "M" which refers to the local time stepping algorithm (see [5] for further details on the local time stepping adaptation). We also note the cpu time
  - cpu_g for the uniform (or global) time stepping,
  - cpu_l for the local time stepping .
- We will compare the adaptive numerical solution to the one computed on a uniform fixed grid. To have a coherent support of comparison, the solution on the fixed grid will be computed with $N_{L_{\max}}$ cells. $N_{L_{\max}}$ stands for the average number of cells used during a simulation of an adaptive scheme with a maximum level $L_{\max}$.
- All of the presented results display the density which is positive. Thus, for the convenience of the reader, in all figures the numerical density of entropy production is plotted with the reversed sign to overlap with the density.

[1] Intel(R) Core(TM) i5-2500 CPU @ 3.30GHz

- For all numerical tests, the initial mesh is adapted to the initial data during few iterations (except for the numerical solution computed on uniform fixed grid) and we have used the following threshold parameters:

$$\begin{array}{lcl} \text{Mesh refinement parameter } \alpha_{\max} & : & 0.01\ , \\ \text{Mesh coarsening parameter } \alpha_{\min} & : & 0.001\ , \\ \text{Mesh refinement parameter } \bar{S} & : & \dfrac{1}{|\Omega|}\displaystyle\sum_{k_b} S^n_{k_b}\ . \end{array}$$

- For each test 1 – test 5, X_{ex} will make reference to the exact solution of the Riemann problem computed using 5 000 uniform cells. For test 6, we use the notation X_{ref} which stands for the reference solution computed on a fixed grid with 20 000 cells using the RK2 scheme.

- To study the numerical convergence of AB1,AB1U, AB1M, RK2U, AB2U, AB2M and RK2 schemes, we have used the discrete l^1_x-norm of the density, momentum, pressure and the internal energy error. We generally used the convergence rate of the internal energy which is more representative of the efficiency of the scheme especially for low density flows.

- On the tables of performance 1, 4, 7, 10, 13 and 16, since the error of the AB1 and AB1M schemes are similar, we only use the results of the AB1 scheme. We also use the AB2 scheme results for the table of performance 2, 5, 8, 11, 14 and 17.

4.1 Test 1: a modified version of the Sod's shock tube problem

We first consider a modified version of the popular Sod's test [17] (see also [5]) which models the one-dimensional flow resulting from the rupture of a membrane separating air with different density/pressure inside a shock tube with a null speed. Besides the fact that the exact solution can be easily computed, the solution of the modified Sod's shock tube problem consists of a right shock wave, a right traveling contact wave and a left sonic rarefaction wave. This is useful to test the ability of the scheme to preserve in-cell entropy inequality even if the adaptive strategy is used.

The test is given by a one-dimensional Riemann problem with the following data:

$$x \in [-1,1], \quad (\rho,u,p)(0,x) = \left\{ \begin{array}{lll} (1, & 0.75, & 1), \quad x \leqslant 0, \\ (0.125, & 0, & 0.1), \quad x > 0\ . \end{array} \right.$$

The computational domain here is $[-1,1]$ with prescribed free boundary conditions.

For each numerical computation, the following parameters have been used:

$$\begin{array}{lcl} \text{CFL} & : & 0.25, \\ \text{Simulation time } (s) & : & 0.2, \\ \text{Initial number of cells} & : & 200, \\ \text{Maximum level of mesh refinement} & : & L_{\max}. \end{array}$$

In figure 2, we display the solution profiles (as well as the exact one) for the density (figure 2(a)), the pressure (figure 2(b)), the momentum (figure 2(c)) and the internal energy (figure 2(d)) of the numerical solution computed with the first order scheme AB1U and AB1 computed with $L_{\max} = 5$. The numerical density of entropy production (S^n_k) is also plotted on figure 2(a).

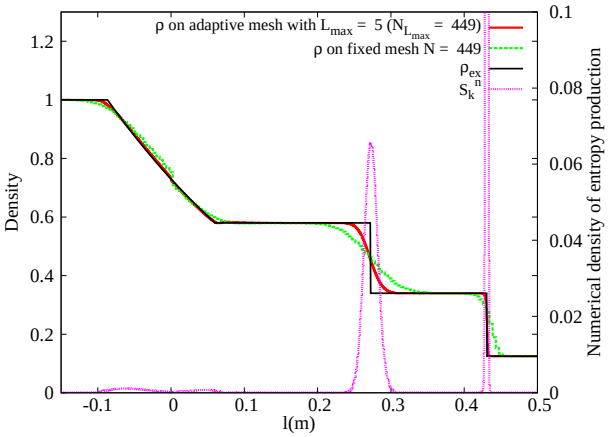

(a) Density and numerical density of entropy production.

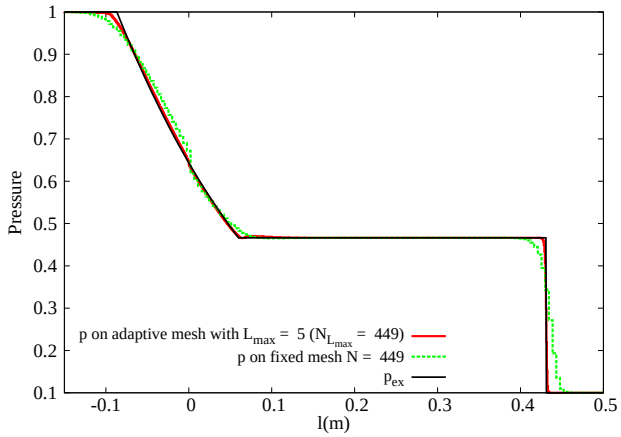

(b) Pressure.

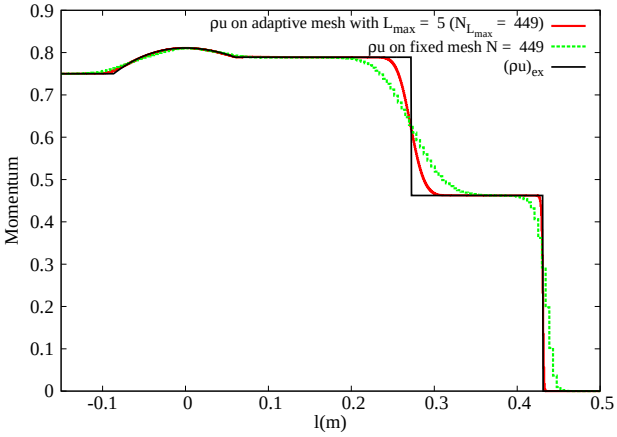

(c) Momentum.

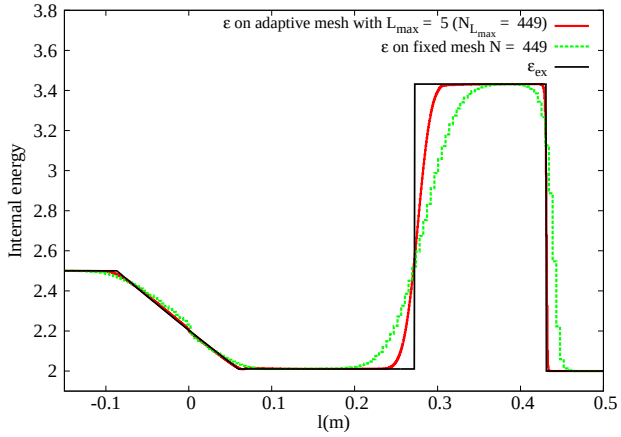

(d) Internal energy.

Figure 2: Test 1: numerical solution at time $t = 0.2$ s with $L_{\max} = 5$ computed with the AB1 scheme.

As usual, by the use of the Godunov solver, the shock wave is rather well-computed with a smearing effects over neighborhood cells for the solution on a fixed grid while it perfectly match when the adaptive grid technique is used (as observed for each state $(\rho, u, p, \varepsilon)$ on figure 2). The numerical diffusion decreases when the solution is refined in around the shock wave as predicted by the numerical density of entropy production, see figure 2(a). Let us also add that no spurious oscillations are observed in the vicinity of the shock when the adaptive grid strategy is used. For more details we refer to [5, Section 5.1.1.].

The contact discontinuity, which is much more difficult to resolve accurately, is here efficiently computed with an adaptive grid since the mesh is well-refined. Another positive feature of the numerical approximation is that the speed of the contact discontinuity is correct for the solution on an adaptive grid even if we use the Osher-Sanders projections which is well-known to be locally non conservative and non consistent (see [14] and [5], since the correct speed of propagation of contact discontinuities are well-computed when the scheme is conservative.)

Another feature concerns the rarefaction waves which are smooth flows. In general, any numerical Finite Volume schemes are able to well-approximate this smooth solution except near the head and the tail. Since the numerical density of entropy production is non zero near the head and the tail (see figure 2(a)), the adaptive solution corresponds to a-well-approximation of the exact solution. Moreover, let us note that the so-called entropy glitch (discontinuity inside the rarefaction) is observed only on a fixed grid (see figures

2(a), 2(b) and 2(d)).

In the following, we display on figure 3 the numerical order of convergence using the discrete l_x^1-norm on the error of the internal energy for the first and second order schemes. We also complete the previous results with the l_x^1 error of ρ, p, u and ε on table 1 and 2 computed with the first and the second order scheme. We finally summarize on table 3 all the rate of convergence of all numerical schemes on ρ, p, u and ε.

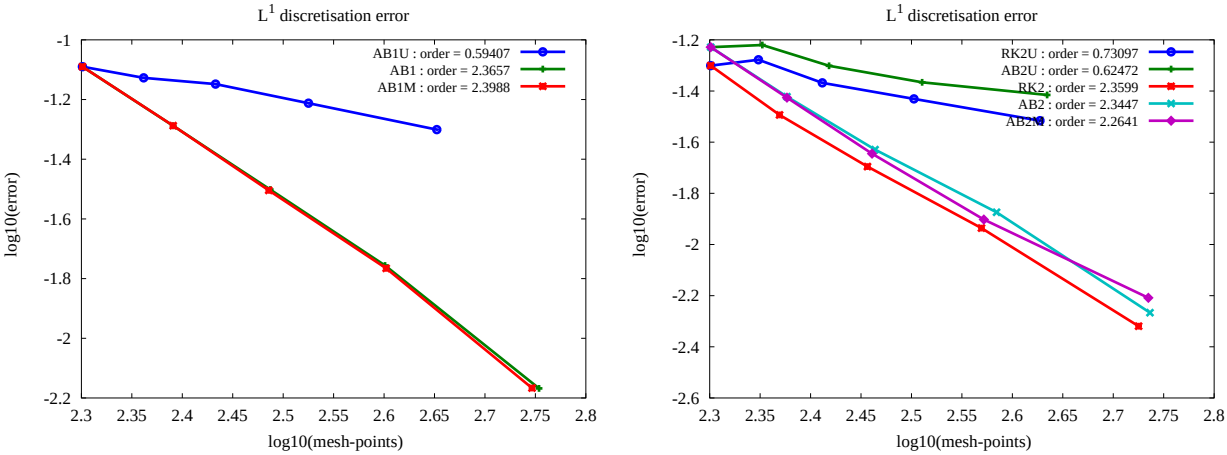

(a) First order scheme.

(b) Second order scheme.

Figure 3: Test 1: $\|\varepsilon - \varepsilon_{ex}\|_{l_x^1}$ with respect to the average number of cells at time $t = 0.2$.

$L_{\max}$	$\|\rho - \rho_{ex}\|_{l_x^1}$	$\|p - p_{ex}\|_{l_x^1}$	$\|u - u_{ex}\|_{l_x^1}$	$\|\varepsilon - \varepsilon_{ex}\|_{l_x^1}$	N_{T_f}	cpu_g	cpu_l
1	0.163E-01	0.112E-01	0.302E-01	0.813E-01	200	0.28	0.28
2	0.103E-01	0.617E-02	0.154E-01	0.515E-01	246	0.66	0.37
3	0.631E-02	0.331E-02	0.761E-02	0.315E-01	307	1.66	0.66
4	0.354E-02	0.167E-02	0.345E-02	0.175E-01	399	3.18	1.36
5	0.142E-02	0.653E-03	0.121E-02	0.679E-02	567	7.37	3.85

Table 1: Test 1 : Convergence tests for first order AB1 scheme, l_x^1-norm at final time with respect to the averaged number of cells $N_{L_{\max}}$ of ρ, u, p and ε, cpu_g for global time stepping and cpu_l local time stepping, N_{T_f} being the number of cells at the final time.

$L_{\max}$	$\|\rho - \rho_{ex}\|_{l_x^1}$	$\|p - p_{ex}\|_{l_x^1}$	$\|u - u_{ex}\|_{l_x^1}$	$\|\varepsilon - \varepsilon_{ex}\|_{l_x^1}$	N_{T_f}	cpu_g	cpu_l
1	0.116E-01	0.725E-02	0.197E-01	0.591E-01	200	0.26	0.26
2	0.736E-02	0.396E-02	0.101E-01	0.378E-01	238	0.58	0.35
3	0.460E-02	0.219E-02	0.509E-02	0.235E-01	291	1.26	0.64
4	0.265E-02	0.115E-02	0.239E-02	0.134E-01	384	2.82	1.38
5	0.116E-02	0.545E-03	0.998E-03	0.541E-02	545	7.34	4.12

Table 2: Test 1 : Convergence tests for second order AB2 scheme, l_x^1-norm at final time with respect to the averaged number of cells $N_{L_{\max}}$ of ρ, u, p and ε, cpu_g for global time stepping and cpu_l local time stepping, N_{T_f} being the number of cells at the final time.

Rate	$\|\rho-\rho_{ex}\|_{l^1_x}$	$\|p-p_{ex}\|_{l^1_x}$	$\|u-u_{ex}\|_{l^1_x}$	$\|\varepsilon-\varepsilon_{ex}\|_{l^1_x}$
AB1U	0.62	0.76	0.80	0.59
AB1	2.33	2.72	3.08	2.37
AB1M	2.44	2.91	3.19	2.40
RK2U	0.72	0.97	1.11	0.73
AB2U	0.65	0.81	0.86	0.62
RK2	2.27	2.51	2.90	2.36
AB2	2.26	2.54	2.94	2.34
AB2M	2.33	2.59	2.79	2.26

Table 3: Test 1 : Convergence tests for first and second order.

As expected, since the solution is discontinuous, we recover approximately order 1 for the first and second order method on uniform mesh. Moreover, we also get "super-convergence" for first order adaptive schemes (see figure 3(a) and tables 1 and 2) as already obtained in [5] for the internal energy. The computational time is considerably reduced when the local time stepping algorithm is used as observed on table 1 and table 4.

4.2 Test 2: a modified 123 problem

The 123 numerical experiment or the Two-Rarefaction test problem (see for instance [4]) is designed to test the ability of the scheme for low density flows. It consists in two symmetric strong rarefaction waves and a trivial contact wave of zero speed. In this test case, the pressure in the star region (i.e., the between the non-linear waves) is close to zero. As a consequence, it yields to some technical difficulty to find the pressure in the iterative Newton-Raphson procedure if the initial guess is not appropriately chosen. In that case, we have used the guess resulting from a linearized solution based on primitive variables (see [18, Formula 4.47]):

$$p_0 = \max(\alpha, P) \text{ where } P = \frac{1}{2}(p_l + p_r) - \frac{1}{8}(u_l - u_r)(\rho_l + \rho_r)(c_l + c_r)$$

where X_l (resp. X_r) stands for the left (resp. the right) state, $c = \sqrt{\dfrac{(\gamma-1)p}{\rho}}$ for the sonic speed and α is a given tolerance (10^{-12} in the present case).

Instead of using the original test,

$$x \in [-1,1], \quad (\rho,u,p)(0,x) = \begin{cases} (1, & -2, & 0.4), & x \leqslant 0, \\ (1, & 2, & 0.4), & x > 0 \end{cases}$$

we consider the modified one given by the following Riemann data:

$$x \in [-1,1], \quad (\rho,u,p)(0,x) = \begin{cases} (1, & -3, & 0.3), & x \leqslant 0, \\ (1, & 3, & 0.3), & x > 0 \end{cases}$$

where the densities is now close to 10^{-3} (instead of 10^{-1} in the original case).

The computational domain here is $[-1,1]$ with free boundary conditions and for each numerical computation, the following parameters have been used:

CFL	:	0.25,
Simulation time (s)	:	0.15,
Initial number of cells	:	200,
Maximum level of mesh refinement	:	$L_{\max}$.

In figure 4, we display the solution profiles (as well as the exact one) for the density (figure 4(a)), the pressure (figure 4(b)), the momentum (figure 4(c)) and the internal energy (figure 4(d)) of the numerical solution

computed with the first order scheme AB1U and AB1 computed with $L_{\max} = 5$. The numerical density of entropy production (S_k^n) is also plotted on figure 4(a).

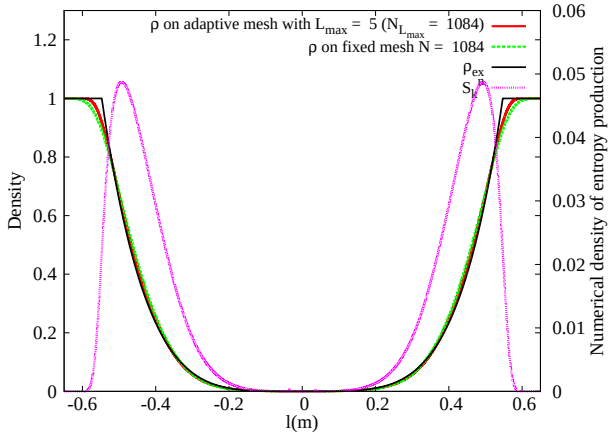

(a) Density and numerical density of entropy production.

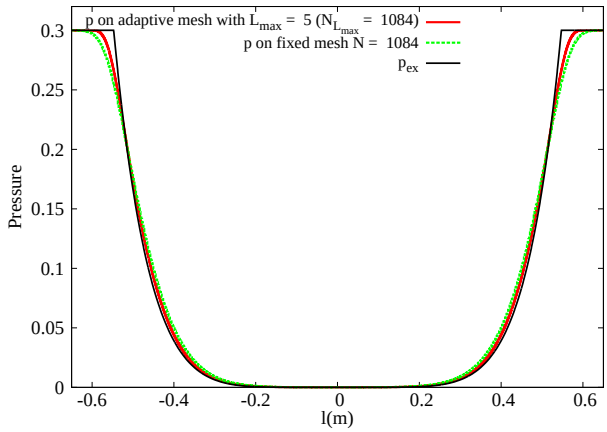

(b) Pressure.

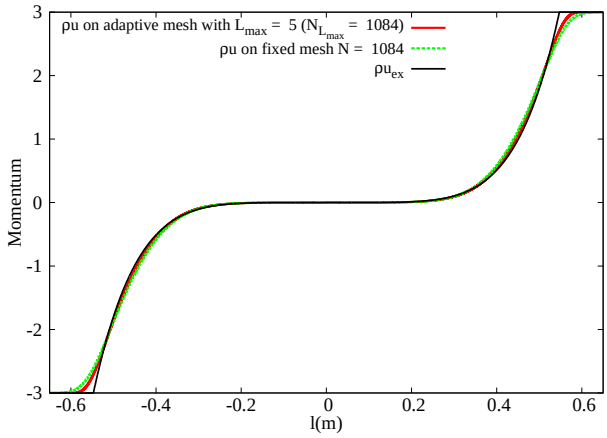

(c) Momentum.

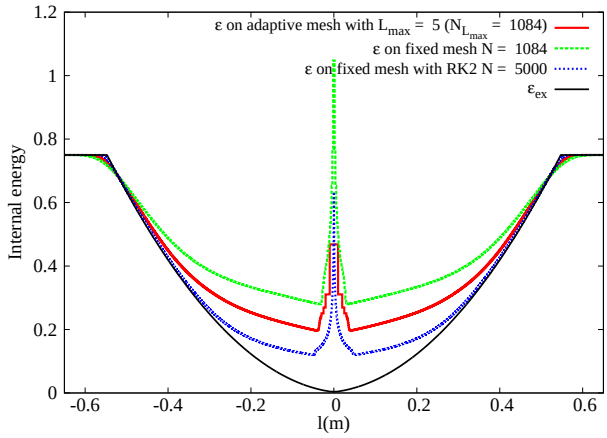

(d) Internal energy.

Figure 4: Test 2: numerical solution at time $t = 0.15$ s with $L_{\max} = 5$ computed with the AB1 scheme.

As pointed out in [18], the Godunov's solver is generally accurate as regards of the primitive variables and even better with the adaptive strategy. Nevertheless, it is no more true when we look for the specific internal energy,

$$\varepsilon = \frac{p}{(\gamma - 1)\rho} ,$$

as one can observe on figure 4(d). We also plot the solution given by the RK2 scheme (which is well-known to be accurate) using 5 000 uniform cells on figure 4(d).

Even in presence of strong rarefactions (see figures 4(a) and 4(b)), the numerical density of entropy production is non zero and thus as pointed out in the previous section, except the head and the tail of the rarefaction, the solution is rather well-computed and even more in the adaptive framework (both from ρ, ρu, p and ε).

Let us also emphasize that in the present adaptive scheme, besides the particular guess in the iterative scheme for finding p, we do not make specific treatment when the solution is close to the vacuum. In

particular, in the low density area, the numerical density of entropy production almost vanishes as shown in figure 4(a).

As done in the previous section, we now complete the previous results with table of performances 4-5 and 6 as well as the rate of convergence of the first and the second order schemes for the internal energy, see figure 5.

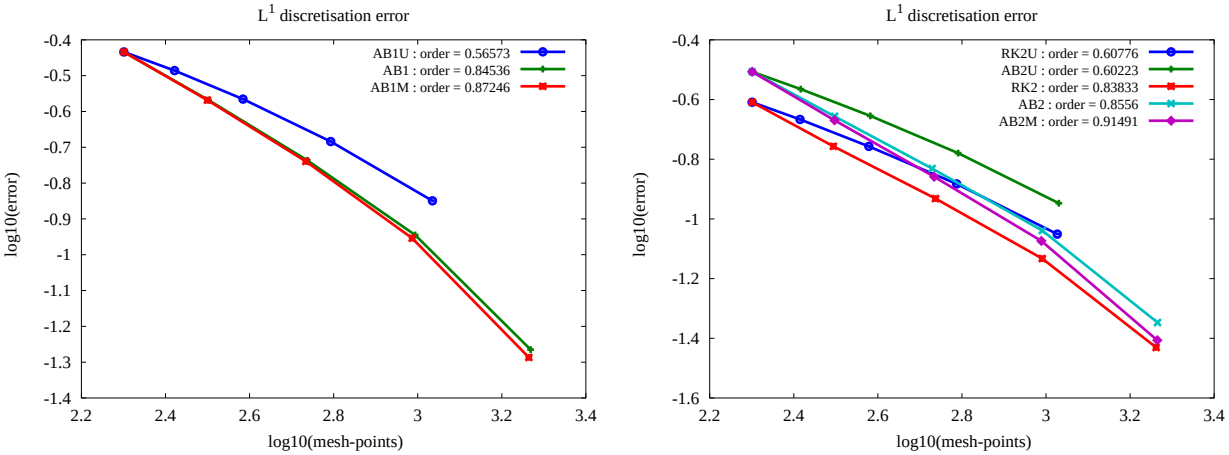

(a) First order scheme.

(b) Second order scheme.

Figure 5: Test 2: $\|\varepsilon - \varepsilon_{ex}\|_{l^1_x}$ with respect to the average number of cells at time $t = 0.15$.

$L_{\max}$	$\|\rho - \rho_{ex}\|_{l^1_x}$	$\|p - p_{ex}\|_{l^1_x}$	$\|u - u_{ex}\|_{l^1_x}$	$\|\varepsilon - \varepsilon_{ex}\|_{l^1_x}$	N_{T_f}	cpu_g	cpu_l
1	0.451E-01	0.214E-01	0.233E+00	0.368E+00	200	0.20	0.20
2	0.290E-01	0.137E-01	0.161E+00	0.270E+00	318	0.57	0.43
3	0.181E-01	0.822E-02	0.125E+00	0.184E+00	546	1.67	1.26
4	0.104E-01	0.435E-02	0.827E-01	0.114E+00	986	6.00	4.97
5	0.403E-02	0.156E-02	0.359E-01	0.543E-01	1856	22.57	19.68

Table 4: Test 2 : Convergence tests for first order AB1 scheme, l^1_x-norm at final time with respect to the averaged number of cells $N_{L_{\max}}$ of ρ, u, p and ε, cpu_g for global time stepping and cpu_l local time stepping, N_{T_f} being the number of cells at the final time.

$L_{\max}$	$\|\rho - \rho_{ex}\|_{l^1_x}$	$\|p - p_{ex}\|_{l^1_x}$	$\|u - u_{ex}\|_{l^1_x}$	$\|\varepsilon - \varepsilon_{ex}\|_{l^1_x}$	N_{T_f}	cpu_g	cpu_l
1	0.357E-01	0.169E-01	0.189E+00	0.311E+00	200	0.20	0.20
2	0.231E-01	0.106E-01	0.154E+00	0.221E+00	314	0.56	0.44
3	0.147E-01	0.630E-02	0.112E+00	0.148E+00	536	1.81	1.44
4	0.853E-02	0.337E-02	0.701E-01	0.914E-01	980	6.40	5.38
5	0.340E-02	0.125E-02	0.309E-01	0.449E-01	1842	22.98	19.85

Table 5: Test 2 : Convergence tests for second order AB2 scheme, l^1_x-norm at final time with respect to the averaged number of cells $N_{L_{\max}}$ of ρ, u, p and ε, cpu_g for global time stepping and cpu_l local time stepping, N_{T_f} being the number of cells at the final time.

Rate	$\|\rho - \rho_{ex}\|_{l^1_x}$	$\|p - p_{ex}\|_{l^1_x}$	$\|u - u_{ex}\|_{l^1_x}$	$\|\varepsilon - \varepsilon_{ex}\|_{l^1_x}$
AB1U	0.69	0.74	0.47	0.57
AB1	1.05	1.15	0.79	0.85
AB1M	1.09	1.18	0.85	0.87
RK2U	0.70	0.81	0.45	0.61
AB2U	0.69	0.77	0.47	0.60
RK2	0.97	1.11	0.76	0.84
AB2	1.03	1.15	0.80	0.86
AB2M	1.08	1.20	0.88	0.91

Table 6: Test 2 : Convergence tests for first and second order.

As expected, the numerical order of the adaptive scheme are better but we do not observe a specific "super-convergence" since no discontinuities are available in the density. Let us also add that the behavior of the internal energy (see figure 4(d)) can be explained by the fact that the density converges faster than the pressure to 0.

4.3 Test 3: the left half of the blast wave of Woodward and Colella

We now focus on a very severe test problem. This test is designed to assess the efficiency of the numerical scheme when the solution contains a strong right shock, a left rarefaction and a contact surface. One can also regard this test problem as the left half of the blast wave problem of Woodward and Colella [20] (see also Test 6).

The test 3 is given by the use of the following Riemann data:

$$x \in [-1,1], \quad (\rho,u,p)(0,x) = \begin{cases} (1, & 0, & 1000), & x \leqslant 0, \\ (1, & 0, & 0.01), & x > 0\ . \end{cases}$$

The computational domain here is $[-1,1]$ and we use free boundary conditions. For each numerical computation, we use the following parameters:

CFL	:	0.25,
Simulation time (s)	:	0.02,
Initial number of cells	:	200,
Maximum level of mesh refinement	:	$L_{\max}$.

In figure 6, we display the solution profiles (as well as the exact one) for the density (figure 6(a)), the pressure (figure 6(b)), the momentum (figure 6(c)) and the internal energy (figure 6(d)) of the numerical solution computed with the first order scheme AB1U and AB1 computed with $L_{\max} = 5$. The numerical density of entropy production (S_k^n) is also plotted on figure 6(a).

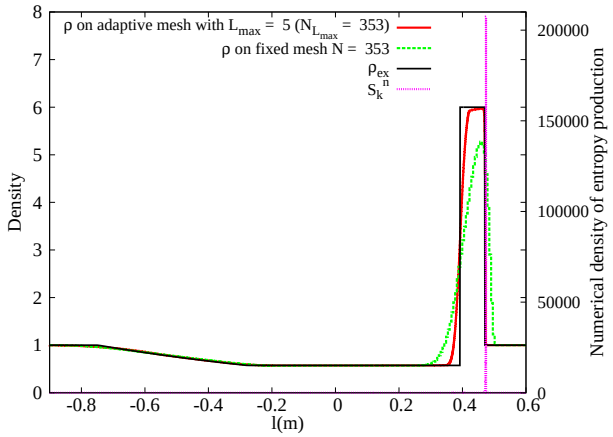

(a) Density and numerical density of entropy production.

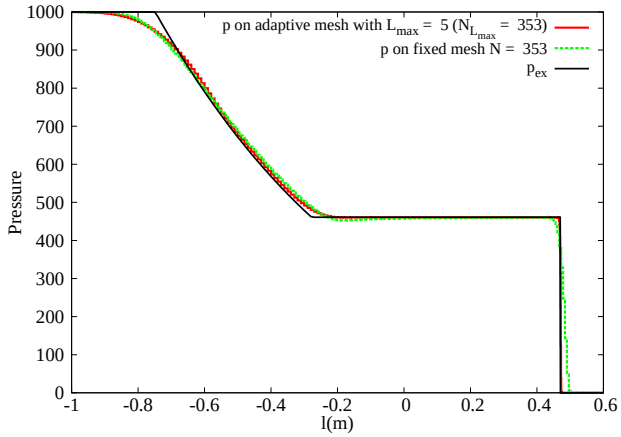

(b) Pressure.

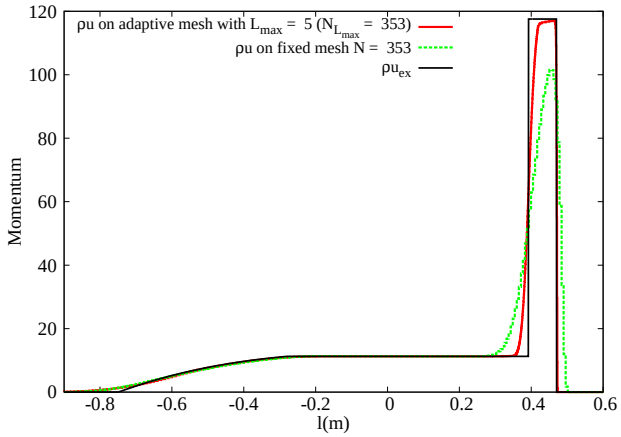

(c) Momentum.

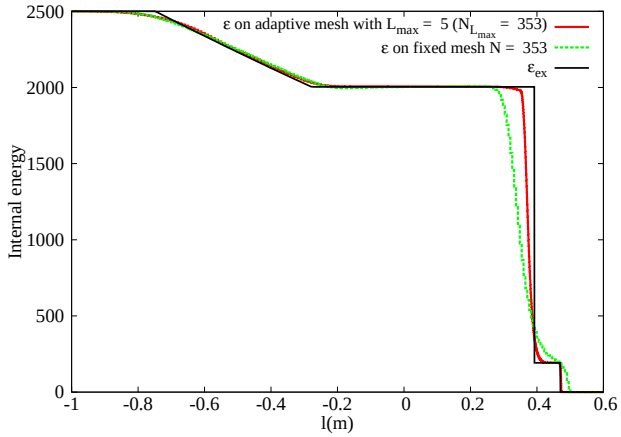

(d) Internal energy.

Figure 6: Test 3: numerical solution at time $t = 0.02$ s with $L_{\max} = 5$ computed with the AB1 scheme.

Even if the solution contains a non physical large shock, this severe test case allows to numerically show the robustness of the numerical scheme. In particular, it is difficult to capture efficiently the pressure (as well as the density) due to the large amplitude of the shock. To get an accurate approximation of the exact solution, a reasonable number of cells ($N_{L_{\max}} = 353$) is required to well-approximate the post shock as clearly seen on the density figure 6(a), the pressure figure 6(b) and the internal energy figure 6(d) (and even better for second order scheme, see table 7 and 8). As observed on figure 6(d), we expect a "super-convergence" (as in the first test problem). We refer to tables 7, 8 and 9.

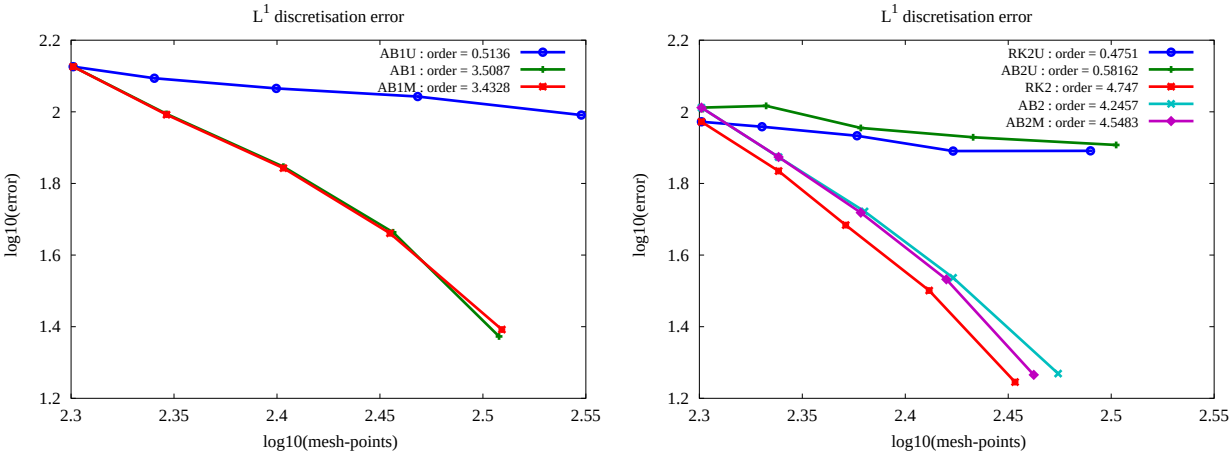

(a) First order scheme.

(b) Second order scheme.

Figure 7: Test 3: $\|\varepsilon - \varepsilon_{ex}\|_{l^1_x}$ with respect to the average number of cells at time $t = 0.02$.

$L_{\max}$	$\|\rho - \rho_{ex}\|_{l^1_x}$	$\|p - p_{ex}\|_{l^1_x}$	$\|u - u_{ex}\|_{l^1_x}$	$\|\varepsilon - \varepsilon_{ex}\|_{l^1_x}$	N_{T_f}	cpu_g	cpu_l
1	0.329E+00	0.268E+02	0.119E+01	0.134E+03	200	0.37	0.36
2	0.225E+00	0.201E+02	0.830E+00	0.986E+02	222	0.78	0.47
3	0.142E+00	0.153E+02	0.590E+00	0.703E+02	253	1.74	0.75
4	0.819E-01	0.123E+02	0.445E+00	0.461E+02	286	4.06	1.50
5	0.345E-01	0.967E+01	0.338E+00	0.236E+02	322	9.64	3.50

Table 7: Test 3 : Convergence tests for first order AB1 scheme, l^1_x-norm at final time with respect to the averaged number of cells $N_{L_{\max}}$ of ρ, u, p and ε, cpu_g for global time stepping and cpu_l local time stepping, N_{T_f} being the number of cells at the final time.

$L_{\max}$	$\|\rho - \rho_{ex}\|_{l^1_x}$	$\|p - p_{ex}\|_{l^1_x}$	$\|u - u_{ex}\|_{l^1_x}$	$\|\varepsilon - \varepsilon_{ex}\|_{l^1_x}$	N_{T_f}	cpu_g	cpu_l
1	0.252E+00	0.182E+02	0.813E+00	0.103E+03	200	0.38	0.39
2	0.164E+00	0.131E+02	0.540E+00	0.747E+02	218	0.82	0.48
3	0.103E+00	0.103E+02	0.390E+00	0.527E+02	240	1.75	0.74
4	0.600E-01	0.865E+01	0.311E+00	0.344E+02	265	3.83	1.38
5	0.261E-01	0.794E+01	0.276E+00	0.186E+02	298	8.80	2.72

Table 8: Test 3 : Convergence tests for second order AB2 scheme, l^1_x-norm at final time with respect to the averaged number of cells $N_{L_{\max}}$ of ρ, u, p and ε, cpu_g for global time stepping and cpu_l local time stepping, N_{T_f} being the number of cells at the final time.

Rate	$\|\rho - \rho_{ex}\|_{l^1_x}$	$\|p - p_{ex}\|_{l^1_x}$	$\|u - u_{ex}\|_{l^1_x}$	$\|\varepsilon - \varepsilon_{ex}\|_{l^1_x}$
AB1U	0.54	0.76	0.78	0.51
AB1	4.58	2.10	2.60	3.51
AB1M	4.50	1.96	2.47	3.43
RK2U	0.69	0.97	1.10	0.48
AB2U	0.53	0.69	0.68	0.58
RK2	6.34	1.86	2.62	4.75
AB2	5.60	2.06	2.69	4.25
AB2M	5.87	2.33	3.04	4.55

Table 9: Test 3 : Convergence tests for first and second order.

4.4 Test 4: the Two Shock Riemann problem

As the test 3, test 4 is also a severe test. The solution is composed of three strong discontinuities (two shocks and a contact discontinuity) traveling to the right. The left shock has a small positive propagation speed while the right is the fastest wave.

The Riemann data are here:

$$x \in [-1,1], \quad (\rho,u,p)(0,x) = \begin{cases} (5.99924, & 19.5975, & 460.894), & x \leqslant 0, \\ (5.99242, & -6.19633, & 46.095), & x > 0\ . \end{cases}$$

The computational domain here is $[-1,1]$ and we use free boundary conditions. For each numerical computation, we use the following parameters:

CFL	:	0.25,
Simulation time (s)	:	0.035,
Initial number of cells	:	200,
Maximum level of mesh refinement	:	$L_{\max}$.

In figure 8, we display the solution profiles (as well as the exact one) for the density (figure 8(a)), the pressure (figure 8(b)), the momentum (figure 8(c)) and the internal energy (figure 8(d)) of the numerical solution computed with the first order scheme AB1U and AB1 computed with $L_{\max} = 5$. The numerical density of entropy production (S_k^n) is also plotted on figure 8(a).

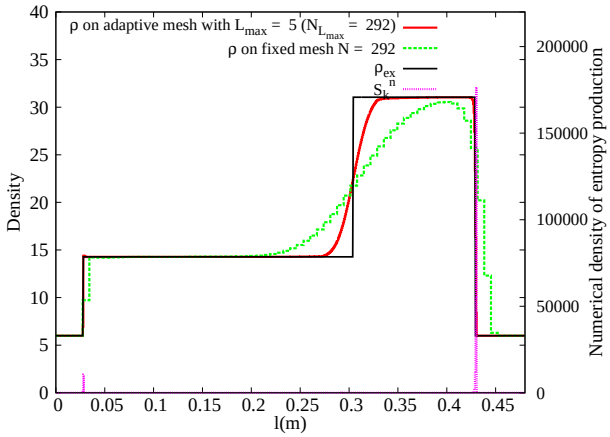

(a) Density and numerical density of entropy production.

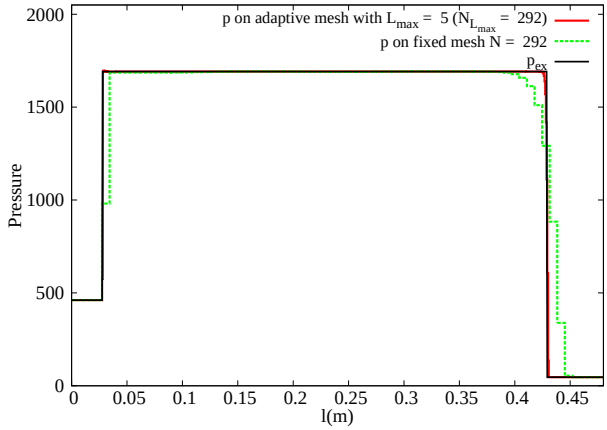

(b) Pressure.

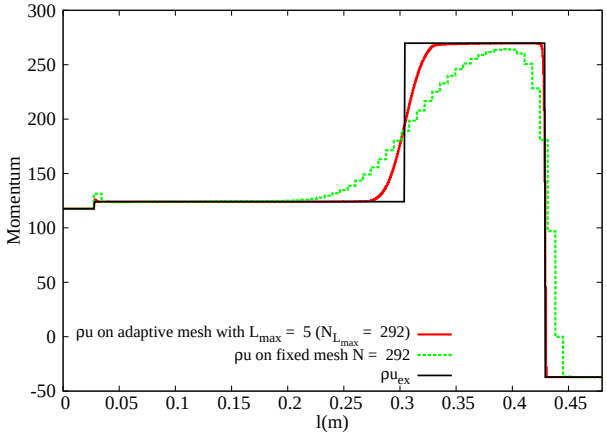

(c) Momentum.

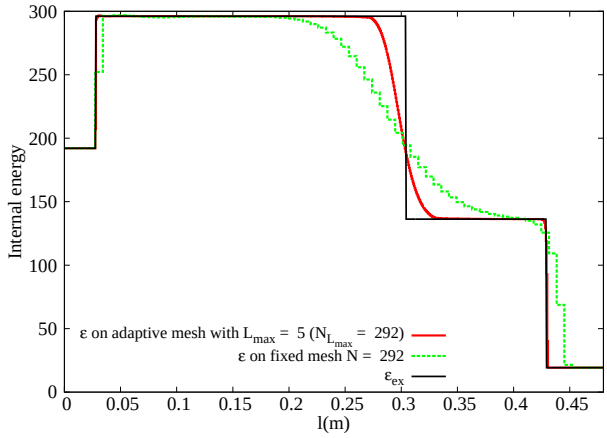

(d) Internal energy.

Figure 8: Test 4: numerical solution at time $t = 0.035$ s with $L_{\max} = 5$ computed with the AB1 scheme.

Even if the left shock wave is very well-resolved, the right one (which is the fastest wave) is smeared over several cells while the numerical diffusion for the contact discontinuity is important. The smearing effects can be reduced with the adaptive scheme since in that case the numerical density entropy production detects the presence of huge discontinuities (see figures 8(a) and 8(d)) and therefore the mesh is refined. Let us also note the presence of spurious oscillations in the slowly moving left shock which are considerably reduced in the adaptive framework (see figure 8(c)). As in the previous test case, the rate of convergence (see table 12) as well as the table of performance (see table 10 and table 11) are exceptional since only 300 cells are used.

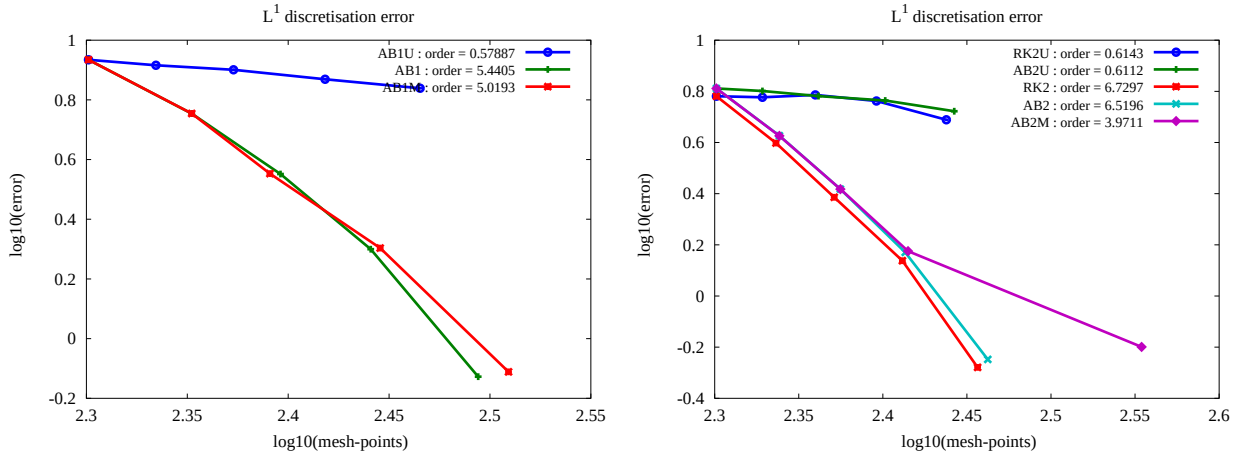

(a) First order scheme.

(b) Second order scheme.

Figure 9: Test 4: $\|\varepsilon - \varepsilon_{ex}\|_{l_x^1}$ with respect to the average number of cells at time $t = 0.035$.

$L_{\max}$	$\|\rho - \rho_{ex}\|_{l_x^1}$	$\|p - p_{ex}\|_{l_x^1}$	$\|u - u_{ex}\|_{l_x^1}$	$\|\varepsilon - \varepsilon_{ex}\|_{l_x^1}$	N_{T_f}	cpu_g	cpu_l
1	0.103E+01	0.266E+02	0.279E+00	0.860E+01	200	0.34	0.34
2	0.641E+00	0.134E+02	0.142E+00	0.568E+01	225	0.72	0.43
3	0.389E+00	0.674E+01	0.687E-01	0.356E+01	249	1.61	0.66
4	0.211E+00	0.270E+01	0.300E-01	0.199E+01	276	3.60	1.23
5	0.794E-01	0.779E+00	0.953E-02	0.745E+00	312	7.78	3.15

Table 10: Test 4 : Convergence tests for first order AB1 scheme, l_x^1-norm at final time with respect to the averaged number of cells $N_{L_{\max}}$ of ρ, u, p and ε, cpu_g for global time stepping and cpu_l local time stepping, N_{T_f} being the number of cells at the final time.

$L_{\max}$	$\|\rho - \rho_{ex}\|_{l_x^1}$	$\|p - p_{ex}\|_{l_x^1}$	$\|u - u_{ex}\|_{l_x^1}$	$\|\varepsilon - \varepsilon_{ex}\|_{l_x^1}$	N_{T_f}	cpu_g	cpu_l
1	0.732E+00	0.175E+02	0.185E+00	0.648E+01	200	0.36	0.36
2	0.461E+00	0.929E+01	0.985E-01	0.423E+01	218	0.78	0.46
3	0.281E+00	0.471E+01	0.470E-01	0.262E+01	237	1.72	0.69
4	0.153E+00	0.197E+01	0.223E-01	0.148E+01	259	3.62	1.25
5	0.579E-01	0.679E+00	0.881E-02	0.565E+00	290	7.97	4.18

Table 11: Test 4 : Convergence tests for second order AB2 scheme, l_x^1-norm at final time with respect to the averaged number of cells $N_{L_{\max}}$ of ρ, u, p and ε, cpu_g for global time stepping and cpu_l local time stepping, N_{T_f} being the number of cells at the final time.

Rate	$\|\rho - \rho_{ex}\|_{l^1_x}$	$\|p - p_{ex}\|_{l^1_x}$	$\|u - u_{ex}\|_{l^1_x}$	$\|\varepsilon - \varepsilon_{ex}\|_{l^1_x}$
AB1U	0.66	0.92	0.94	0.58
AB1	5.71	7.93	7.60	5.44
AB1M	5.29	6.71	6.64	5.02
RK2U	0.46	0.66	0.58	0.61
AB2U	0.69	1.07	1.25	0.61
RK2	6.99	9.00	8.44	6.73
AB2	6.79	8.81	8.28	6.52
AB2M	4.01	3.98	4.41	3.97

Table 12: Test 4 : Convergence tests for first and second order.

4.5 Test 5: a modified Leblanc test problem

We present in this section a modified version of the so-called Leblanc test problem which is an extreme shock tube problem. The initial discontinuity separates a region of very high energy and density from one of low energy and density. This is a much more severe test than the Sod Problem. The solution consists of a rarefaction moving to the left, and a contact discontinuity and a strong shock moving to the right.

The Riemann data for this test problem are:

$$x \in [-1,1], \quad (\rho,u,p)(0,x) = \begin{cases} (1, & 0, & 0.1), & x \leqslant 0, \\ (0.001, & 0, & 10^{-9}), & x > 0\ . \end{cases}$$

The computational domain here is $[-1,1]$ with prescribed free boundary conditions and we have used the following parameters:

CFL	:	0.25,
Simulation time (s)	:	0.7,
Initial number of cells	:	200,
Maximum level of mesh refinement	:	$L_{\max}$.

In figure 10, we display the solution profiles (as well as the exact one) for the density (figure 10(a)), the pressure (figure 10(b)), the momentum (figure 10(c)) and the internal energy (figure 10(d)) of the numerical solution computed with the first order scheme AB1U and AB1 computed with $L_{\max} = 5$. The numerical density of entropy production (S_k^n) is also plotted on figure 10(a).

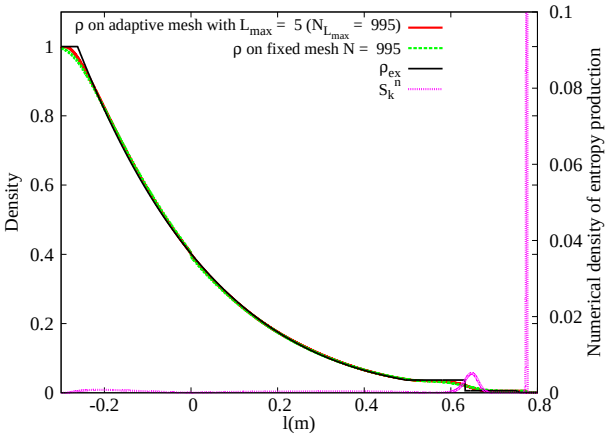

(a) Density and numerical density of entropy production.

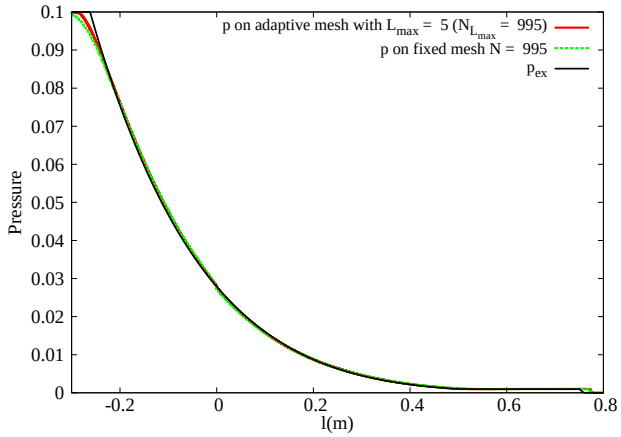

(b) Pressure.

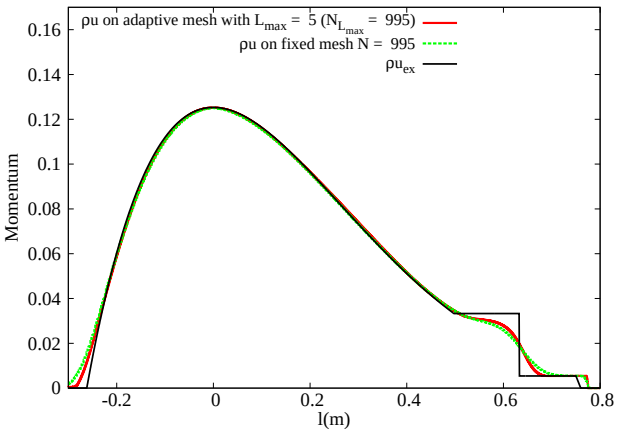

(c) Momentum.

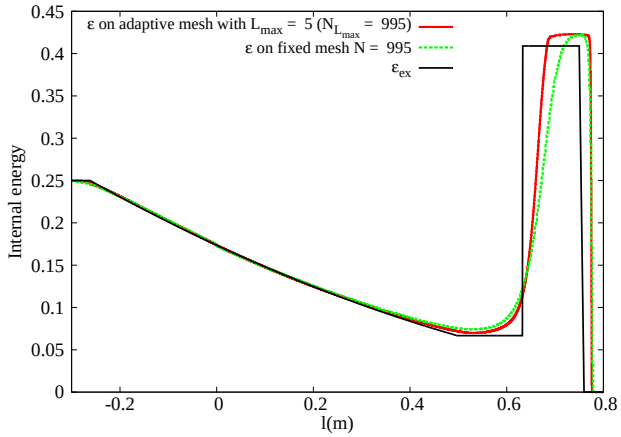

(d) Internal energy.

Figure 10: Test 5: numerical solution at time $t = 0.7$ s with $L_{\max} = 5$ computed with the AB1 scheme.

This modified test is a challenging test problem since the presence of the strong left rarefaction wave and discontinuities of small amplitude make it difficult. Indeed, while the speed of the contact discontinuity is correct, we make an error on the correct shock speed as one can observe on figures 10(c) and 10(d) when the number of cells is approximately 1 000 cells. As a consequence, the post shock values are extrapolated (see, 10(d)) even if the contact discontinuity and the speed of propagation of the rarefaction are well-computed.

Starting with 500 cells instead of 200 cells, we get better results as displayed on figure 11(d). This behavior is not due to a lack of accuracy of the present scheme but it is due to the extreme difficulty of this test problem. Let us note that in the literature for the original Leblanc test problem, they generally use more than 3 000 cells with high order scheme to resolve it “accurately”.

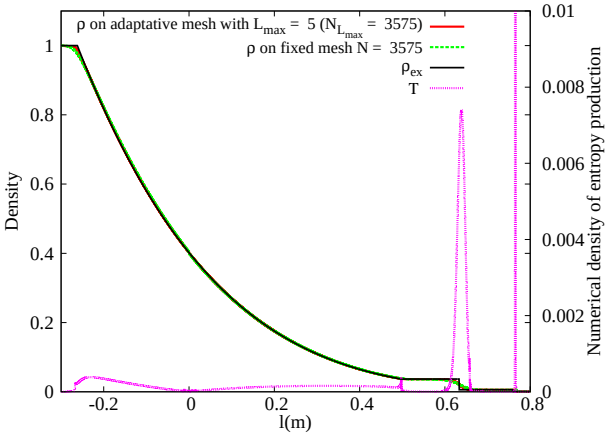

(a) Density and numerical density of entropy production.

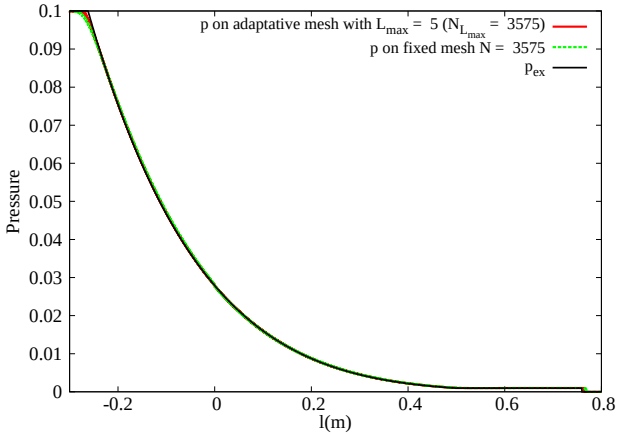

(b) Pressure.

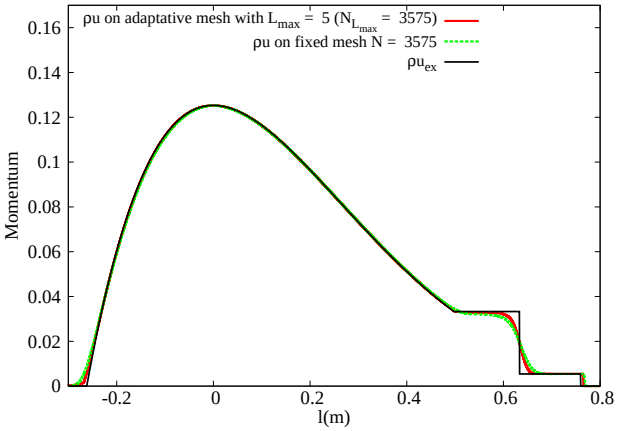

(c) Momentum.

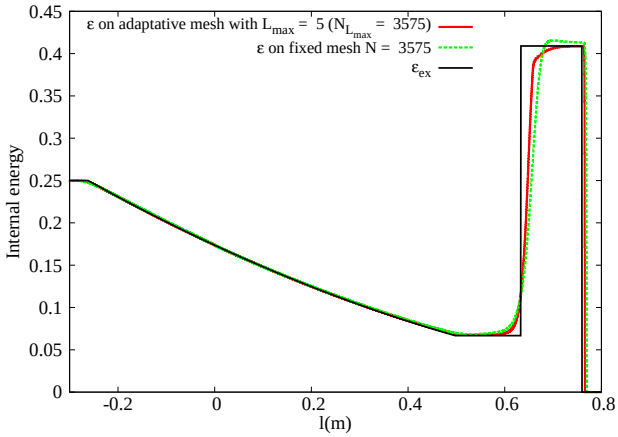

(d) Internal energy.

Figure 11: Test 5: numerical solution at time $t = 0.7$ s with $L_{\max} = 5$ computed with the AB1 scheme with 500 cells.

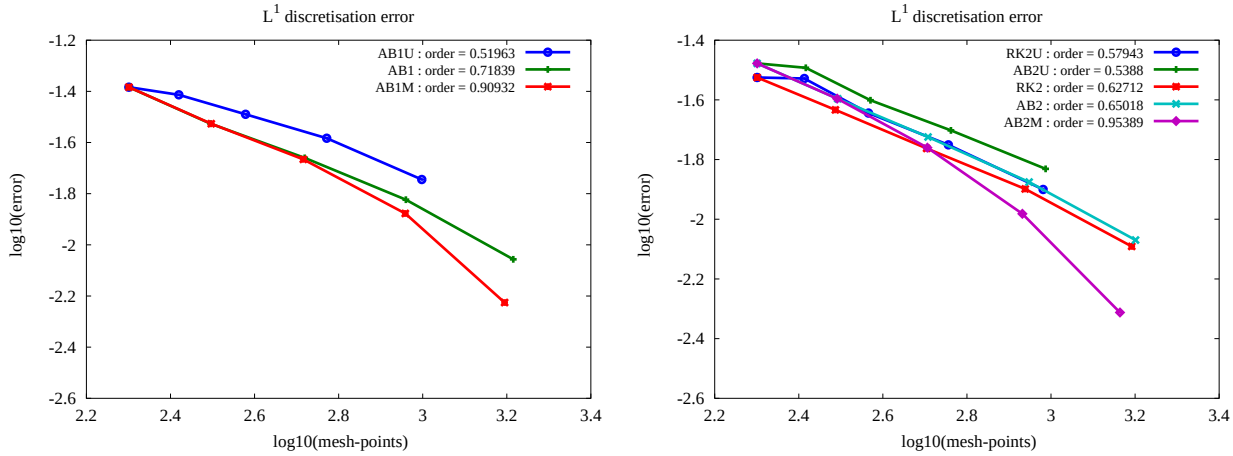

(a) First order scheme.

(b) Second order scheme.

Figure 12: Test 5: $\|\varepsilon - \varepsilon_{ex}\|_{l^1_x}$ with respect to the average number of cells at time $t = 0.15$.

$L_{\max}$	$\|\rho - \rho_{ex}\|_{l^1_x}$	$\|p - p_{ex}\|_{l^1_x}$	$\|u - u_{ex}\|_{l^1_x}$	$\|\varepsilon - \varepsilon_{ex}\|_{l^1_x}$	N_{T_f}	cpu_g	cpu_l
1	0.151E-01	0.166E-02	0.390E-01	0.413E-01	200	0.30	0.31
2	0.964E-02	0.102E-02	0.271E-01	0.298E-01	313	0.92	0.74
3	0.601E-02	0.599E-03	0.209E-01	0.219E-01	524	2.98	2.30
4	0.350E-02	0.332E-03	0.157E-01	0.150E-01	912	9.68	7.87
5	0.151E-02	0.138E-03	0.112E-01	0.878E-02	1642	32.13	26.42

Table 13: Test 5 : Convergence tests for first order AB1 scheme, l^1_x-norm at final time with respect to the averaged number of cells $N_{L_{\max}}$ of ρ, u, p and ε, cpu_g for global time stepping and cpu_l local time stepping, N_{T_f} being the number of cells at the final time.

$L_{\max}$	$\|\rho - \rho_{ex}\|_{l^1_x}$	$\|p - p_{ex}\|_{l^1_x}$	$\|u - u_{ex}\|_{l^1_x}$	$\|\varepsilon - \varepsilon_{ex}\|_{l^1_x}$	N_{T_f}	cpu_g	cpu_l
1	0.103E-01	0.106E-02	0.304E-01	0.333E-01	200	0.35	0.35
2	0.680E-02	0.669E-03	0.240E-01	0.253E-01	311	1.03	0.81
3	0.443E-02	0.415E-03	0.189E-01	0.189E-01	510	3.09	2.39
4	0.277E-02	0.250E-03	0.146E-01	0.133E-01	887	9.58	7.67
5	0.132E-02	0.117E-03	0.114E-01	0.852E-02	1589	32.53	25.94

Table 14: Test 5 : Convergence tests for second order AB2 scheme, l^1_x-norm at final time with respect to the averaged number of cells $N_{L_{\max}}$ of ρ, u, p and ε, cpu_g for global time stepping and cpu_l local time stepping, N_{T_f} being the number of cells at the final time.

Rate	$\|\rho - \rho_{ex}\|_{l^1_x}$	$\|p - p_{ex}\|_{l^1_x}$	$\|u - u_{ex}\|_{l^1_x}$	$\|\varepsilon - \varepsilon_{ex}\|_{l^1_x}$
AB1U	0.75	0.84	0.55	0.52
AB1	1.07	1.16	0.58	0.72
AB1M	1.23	1.33	0.84	0.91
RK2U	0.81	0.88	0.64	0.58
AB2U	0.75	0.82	0.57	0.54
RK2	0.95	1.03	0.47	0.63
AB2	0.97	1.04	0.47	0.65
AB2M	1.29	1.37	1.01	0.95

Table 15: Test 5 : Convergence tests for first and second order.

4.6 Test 6: the blast wave problem

The Woodward-Colella blast wave test problem can be extremely difficult to solve on a uniform grid even if we use a very large number of cells. This one-dimensional test problem was initially introduced in [21] and it makes one of the main difficult and the main challenging test case to solve in order to show the efficiency of the numerical method. In particular, it illustrate the strong relationship between the accuracy of the overall flow solution and the thinness of discontinuities on the grid involving multiple interactions of discontinuities (shocks and contact discontinuities) and rarefactions with each other. The initial condition consists of three constant states

$$x \in [-1,1], \rho(0,x) = 1, \quad u(0,x) = 0, \quad p(0,x) = \begin{cases} 1000, & x \leqslant 0.1, \\ 0.01, & 0.1 < x \leqslant 0.9, \\ 100, & x > 0.9\ . \end{cases}$$

on a computational domain $[0,1]$ with prescribed reflecting boundary conditions.

In that case, as a reference solution, we compute the solution on a uniform grid with 20 000 cells using the RK2U scheme. We also use the following parameters:

CFL	:	0.25,
Simulation time (s)	:	0.038,
Initial number of cells	:	200,
Maximum level of mesh refinement	:	$L_{\max}$.

In figure 13, we display the solution profiles (as well as the reference one) for the density (figure 13(a)), the pressure (figure 13(b)), the momentum (figure 13(c)) and the internal energy (figure 13(d)) of the numerical solution computed with the first order scheme AB1U and AB1 computed with $L_{\max} = 5$. The numerical density of entropy production (S_k^n) is also plotted on figure 13(a).

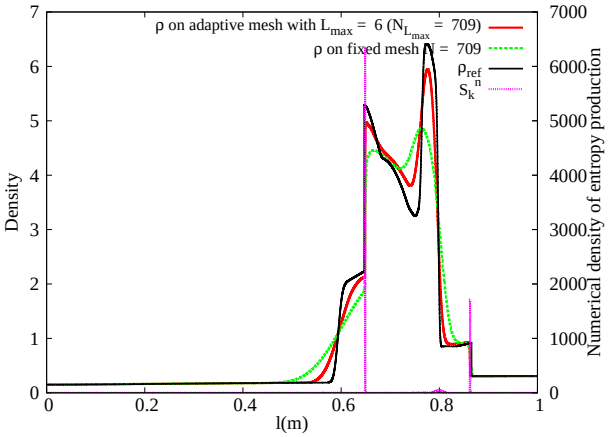

(a) Density and numerical density of entropy production.

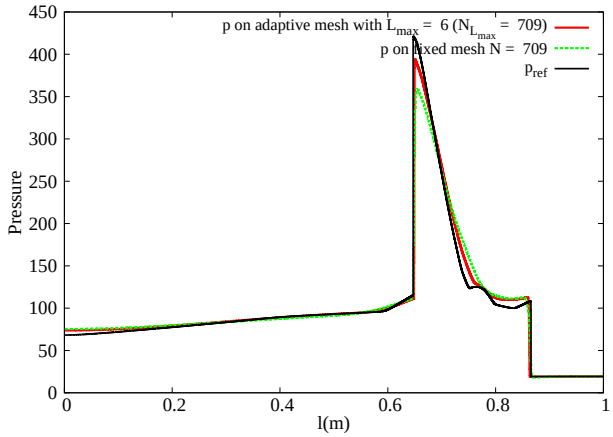

(b) Pressure.

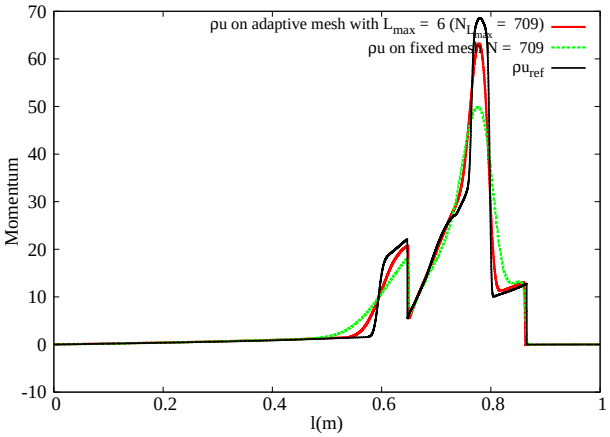

(c) Momentum.

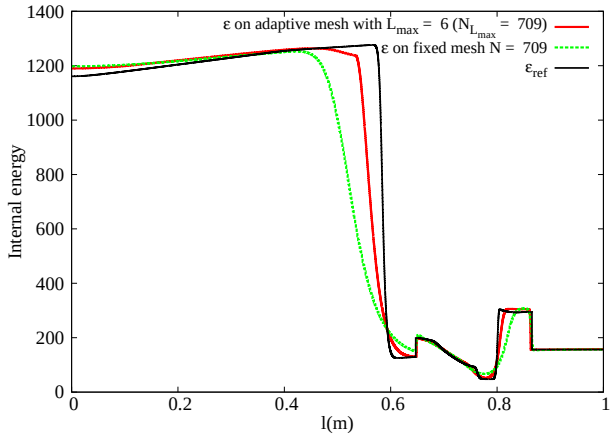

(d) Internal energy.

Figure 13: Test 6: numerical solution at time $t = 0.038$ s with $L_{\max} = 5$ computed with the AB1 scheme.

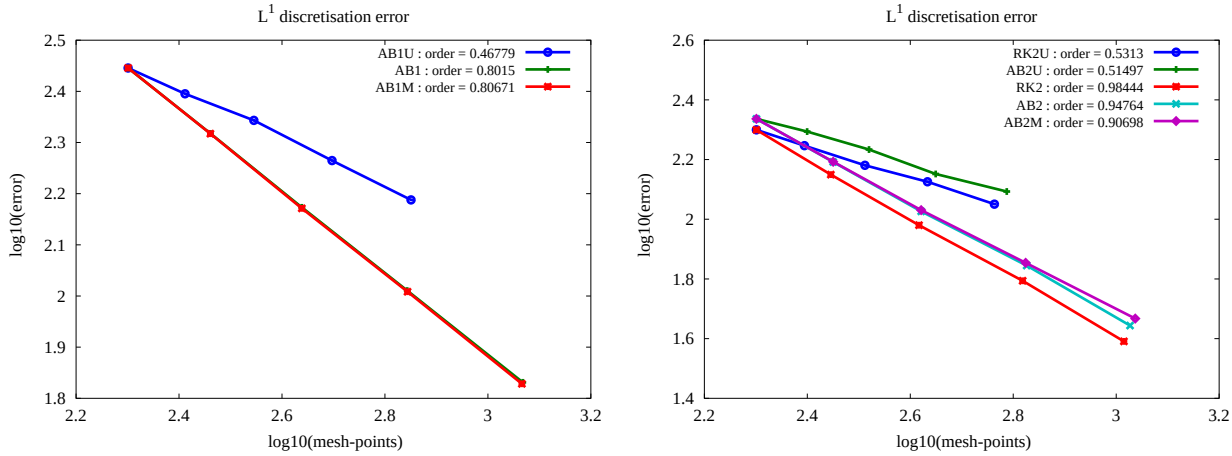

(a) First order scheme.

(b) Second order scheme.

Figure 14: Test 6: $\|\varepsilon - \varepsilon_{ex}\|_{l^1_x}$ with respect to the average number of cells at time $t = 0.038$.

$L_{\max}$	$\|\rho - \rho_{ex}\|_{l^1_x}$	$\|p - p_{ex}\|_{l^1_x}$	$\|u - u_{ex}\|_{l^1_x}$	$\|\varepsilon - \varepsilon_{ex}\|_{l^1_x}$	N_{T_f}	cpu_g	cpu_l
1	0.645E+00	0.259E+02	0.104E+01	0.279E+03	200	1.30	1.30
2	0.528E+00	0.192E+02	0.923E+00	0.208E+03	289	3.38	2.48
3	0.409E+00	0.141E+02	0.801E+00	0.149E+03	435	9.16	6.21
4	0.294E+00	0.104E+02	0.679E+00	0.102E+03	697	25.78	17.61
5	0.197E+00	0.796E+01	0.588E+00	0.678E+02	1169	73.22	50.98

Table 16: Test 6 : Convergence tests for first order AB1 scheme, l^1_x-norm at final time with respect to the averaged number of cells $N_{L_{\max}}$ of ρ, u, p and ε, cpu_g for global time stepping and cpu_l local time stepping, N_{T_f} being the number of cells at the final time.

$L_{\max}$	$\|\rho - \rho_{ex}\|_{l^1_x}$	$\|p - p_{ex}\|_{l^1_x}$	$\|u - u_{ex}\|_{l^1_x}$	$\|\varepsilon - \varepsilon_{ex}\|_{l^1_x}$	N_{T_f}	cpu_g	cpu_l
1	0.548E+00	0.193E+02	0.872E+00	0.217E+03	200	1.31	1.36
2	0.421E+00	0.132E+02	0.706E+00	0.156E+03	282	3.32	2.46
3	0.301E+00	0.929E+01	0.566E+00	0.106E+03	418	8.82	5.64
4	0.202E+00	0.672E+01	0.448E+00	0.700E+02	670	23.64	15.26
5	0.127E+00	0.528E+01	0.396E+00	0.440E+02	1064	65.01	41.86

Table 17: Test 6 : Convergence tests for second order AB2 scheme, l^1_x-norm at final time with respect to the averaged number of cells $N_{L_{\max}}$ of ρ, u, p and ε, cpu_g for global time stepping and cpu_l local time stepping, N_{T_f} being the number of cells at the final time.

Rate	$\|\rho - \rho_{ex}\|_{l^1_x}$	$\|p - p_{ex}\|_{l^1_x}$	$\|u - u_{ex}\|_{l^1_x}$	$\|\varepsilon - \varepsilon_{ex}\|_{l^1_x}$
AB1U	0.35	0.60	0.41	0.47
AB1	0.67	0.67	0.33	0.80
AB1M	0.66	0.68	0.35	0.81
RK2U	0.44	0.70	0.55	0.53
AB2U	0.43	0.65	0.42	0.51
RK2	0.90	0.75	0.48	0.98
AB2	0.87	0.77	0.48	0.95
AB2M	0.77	0.72	0.39	0.91

Table 18: Test 6 : Convergence tests for first and second order.

We numerically show that the adaptive grid strategy using the numerical density of entropy production can considerably increase the accuracy without requiring a large number of cells and without a lot of extra CPU times as required by solving the problem on a uniform grid.

5 Concluding remarks and perspectives

In this paper, we have used the adaptive numerical scheme based on the numerical density of entropy production introduced by Ersoy *et al* [5]. This scheme employs a useful adaptive strategy based on the mathematical (physical) entropy which indicates on the need to refine or to coarsen the mesh, in particular in the presence of strong discontinuities. Moreover, combining into a local time stepping method, one can considerably decrease the computational cost keeping the same order of accuracy. Through several severe test problems for which the solution contains strong discontinuities, strong rarefaction and/or low density, we have numerically shown the robustness of the scheme. Indeed, resulting numerical solutions are both accurate for contact discontinuities and the head/tail of rarefaction waves which are well-known to be difficult to handle numerically.

Acknowledgements

This work is supported by the ModTerCom project within the APEX program of the region Provence-Alpe-Côte d'Azur.

References

[1] M. Berger and J. Oliger, *Adaptive mesh refinement for hyperbolic partial differential equations*, J. Comp. Phys., 53 (1984), pp. 484–512.

[2] G.-Q. Chen, *Vacuum states and global stability of rarefaction waves for compressible flow*, Methods Appl. Anal., 7 (2000), pp. 337–361. Cathleen Morawetz: a great mathematician.

[3] C. M. Dafermos, *Hyperbolic conservation laws in continuum physics*, vol. 325 of Grundlehren der Mathematischen Wissenschaften [Fundamental Principles of Mathematical Sciences], Springer-Verlag, Berlin, third ed., 2010.

[4] B. Einfeldt, C.-D. Munz, P. L. Roe, and B. Sjögreen, *On Godunov-type methods near low densities*, J. Comput. Phys., 92 (1991), pp. 273–295.

[5] M. Ersoy, F. Golay, and L. Yushchenko, *Adaptive multiscale scheme based on numerical density of entropy production for conservation laws*, Cent. Eur. J. Math., 11 (2013), pp. 1392–1415.

[6] T. Gallouët, J.-M. Hérard, and N. Seguin, *Some recent finite volume schemes to compute Euler equations using real gas EOS*, Internat. J. Numer. Methods Fluids, 39 (2002), pp. 1073–1138.

[7] P. Houston, J. Mackenzie, E. Süli, and G. Warnecke, *A posteriori error analysis for numerical approximations of Friedrichs systems*, Numer. Math., 82 (1999), pp. 433–470.

[8] F. Huang and R. Pan, *Convergence rate for compressible Euler equations with damping and vacuum*, Arch. Ration. Mech. Anal., 166 (2003), pp. 359–376.

[9] ——, *Asymptotic behavior of the solutions to the damped compressible Euler equations with vacuum*, J. Differential Equations, 220 (2006), pp. 207–233.

[10] S. Karni and A. Kurganov, *Local error analysis for approximate solutions of hyperbolic conservation laws*, Adv. Comput. Math., 22 (2005), pp. 79–99.

[11] S. Karni, A. Kurganov, and G. Petrova, *A smoothness indicator for adaptive algorithms for hyperbolic systems*, J. Comp. Phys., 178 (2002), pp. 323–341.

[12] L. D. Landau and E. M. Lifshitz, *Fluid mechanics*, Translated from the Russian by J. B. Sykes and W. H. Reid. Course of Theoretical Physics, Vol. 6, Pergamon Press, London, 1959.

[13] R. J. LeVeque, *Finite volume methods for hyperbolic problems*, vol. 31, Cambridge university press, 2002.

[14] S. Osher and R. Sanders, *Numerical approximations to nonlinear conservation laws with locally varying time and space grids*, Math. Comp., 41 (1983), pp. 321–336.

[15] P. L. Sachdev, *Shock waves and explosions*, vol. 132 of Chapman & Hall/CRC Monographs and Surveys in Pure and Applied Mathematics, Chapman & Hall/CRC, Boca Raton, FL, 2004.

[16] D. Serre, *Systems of conservation laws. 1*, Cambridge University Press, Cambridge, 1999. Hyperbolicity, entropies, shock waves, Translated from the 1996 French original by I. N. Sneddon.

[17] G.-A. Sod, *A survey of several finite difference methods for systems of nonlinear hyperbolic conservation laws*, J. Comput. Phys., 27 (1978), pp. 1–31.

[18] E. F. Toro, *Riemann solvers and numerical methods for fluid dynamics*, Springer-Verlag, Berlin, third ed., 2009. A practical introduction.

[19] P. Woodward and P. Colella, *High resolution difference schemes for compressible gas dynamics*, in Seventh International Conference on Numerical Methods in Fluid Dynamics (Stanford Univ., Stanford, Calif.; NASA/Ames Res. Center, Moffett Field, Calif., 1980), vol. 141 of Lecture Notes in Phys., Springer, Berlin, 1981, pp. 434–441.

[20] ——, *The numerical simulation of two-dimensional fluid flow with strong shocks*, J. Comput. Phys., 54 (1984), pp. 115–173.

[21] P. R. Woodward, *Trade-offs in designing explicit hydrodynamical schemes for vector computers*, in Parallel computations, vol. 1 of Comput. Tech., Academic Press, Orlando, FL, 1982, pp. 153–171.

[22] L. Yushchenko, F. Golay, and M. Ersoy, *Entropy production and mesh refinement – Application to wave breaking.*, in Congrès Français de Mécanique, Bordeaux, August, 2013.